Optogenetic Stimulation of Cholinergic Amacrine Cells Improves Capillary Blood Flow in Diabetic Retinopathy

Elena Ivanova,[1,3] Paola Bianchimano,[1] Carlo Corona,[1] Cyril G. Eleftheriou,[1] and Botir T. Sagdullaev[1,2]

[1]Burke Neurological Institute, White Plains, New York, United States
[2]Department of Ophthalmology, Weill Cornell Medicine, New York, United States
[3]Department of Neuroscience, Weill Cornell Medicine, New York, United States

Correspondence: Botir T. Sagdullaev, Burke Neurological Institute, 785 Mamaroneck Avenue, White Plains, NY 10605, USA; bos2005@med.cornell.edu.

Received: May 4, 2020
Accepted: August 5, 2020
Published: August 25, 2020

Citation: Ivanova E, Bianchimano P, Corona C, Eleftheriou CG, Sagdullaev BT. Optogenetic stimulation of cholinergic amacrine cells improves capillary blood flow in diabetic retinopathy. *Invest Ophthalmol Vis Sci.* 2020;61(10):44. https://doi.org/10.1167/iovs.61.10.44

Purpose. Disruption in blood supply to active retinal circuits is the earliest hallmark of diabetic retinopathy (DR) and has been primarily attributed to vascular deficiency. However, accumulating evidence supports an early role for a disrupted neuronal function in blood flow impairment. Here, we tested the hypothesis that selectively stimulating cholinergic neurons could restore neurovascular signaling to preserve the capillary circulation in DR.

Methods. We used wild type (wt) and choline acetyltransferase promoter (ChAT)-channelrhodopsin-2 (ChR2) mice expressing ChR2 exclusively in cholinergic cells. Mice were made diabetic by streptozotocin (STZ) injections. Two to 3 months after the last STZ injection, the rate of capillary blood flow was measured in vivo within each retinal vascular layer using high speed two-photon imaging. Measurements were done at baseline and following ChR2-driven activation of retinal cholinergic interneurons, the sole source of the vasodilating neurotransmitter acetylcholine. After recordings, retinas were collected and assessed for physiological and structural features.

Results. In retinal explants from ChAT-ChR2 mice, we found that channelrhodopsin2 was selectively expressed in all cholinergic amacrine cells. Its direct activation by blue light led to dilation of adjacent retinal capillaries. In living diabetic ChAT-ChR2 animals, basal capillary blood flow was significantly higher than in diabetic mice without channelrhodopsin. However, optogenetic stimulation with blue light did not result in flickering light-induced functional hyperemia, suggesting a necessity for a concerted neurovascular interaction.

Conclusions. These findings provide direct support to the utility and efficacy of an optogenetic approach for targeting selective retinal circuits to treat DR and its complications.

Keywords: diabetic retinopathy, blood flow, optogenetics, cholinergic cells, vascular relay

Impaired retinal blood flow, an early sign of diabetic retinopathy (DR), is thought to be associated with deficits in both neuronal and vascular elements.[1] However, their distinct contributions are not clear. Changes to the retinal vasculature are shown to be a key factor at manifest stages of DR, and accumulating evidence indicates that neuronal signaling is affected much earlier than previously thought.[2] In the retina, blood vessels occupy four distinct laminae, creating spatially and functionally specialized domains that are positioned in the proximity to neurotransmitter release sites (Figs. 1A–D). Specifically, a deep vascular lamina serves the outer plexiform layer, whereas intermediate and sublaminar capillaries nourish the inner plexiform layer.[3] Surrounded by neuronal synapses, capillaries sense neuronal activity and adjust blood flow on demand.[4,5] The retinal arterioles are positioned in the superficial lamina, outside of the synaptic contacts, and rely on a "sensory" signal from the capillaries.

Among the diverse retinal neural networks that participate in neurovascular interactions, the cholinergic system is of particular interest. Acetylcholine (ACh) is a potent vasodilator released by a class of genetically defined cholinergic amacrine cells. The vascular targets of ACh are muscarinic type 3 receptors (m3AChRs) on both endothelial cells and pericytes.[6] However, the action of ACh on each of these cell types remains controversial, with reports of diametrically opposed effects on capillary diameter.[7–10] The potential sites of interaction are also poorly understood, and may include blood vessels in both ON and OFF sublaminae within the inner plexiform layer (IPL; see Fig. 1C). Here, diving capillaries pass through cholinergic synapses in the ON IPL plexus. Downstream, the capillaries within the sublaminar vascular layer appear to be directly targeted by OFF cholinergic cells.[3] Therefore, a strategic placement of cholinergic modulatory elements along transit capillary branches supports their critical role in retina supply. Indeed, a recent analysis of brain vasculature indicated that a significant fraction of the hemodynamic resistance to blood flow lies within a vast capillary network.[11] It is estimated that a 6.7% change in capillary diameter could

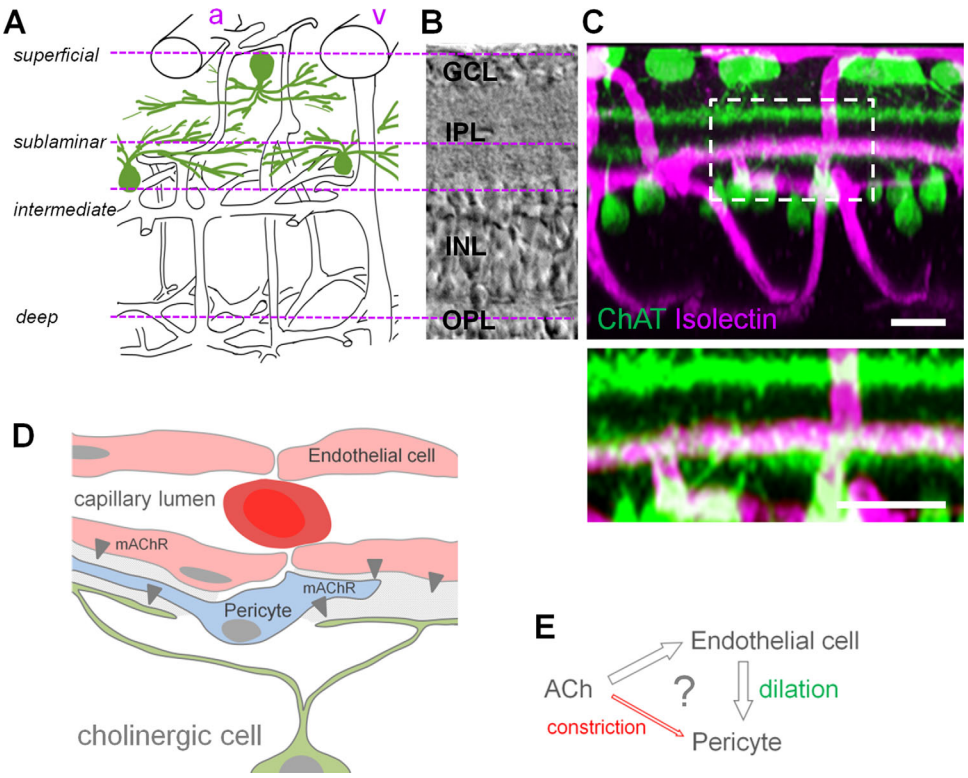

Figure 1. Cholinergic modulation of retinal vasculature. (**A**) Schematic of the laminar neurovascular network showing the first-order arteriole (a) and venule (v) along with the capillaries. Connectivity of the superficial, sublaminar, intermediate, and deep vascular laminae is shown within the retina layers (B). (**B**) Transmitted light image of a vertical cryostat section through the mouse retina. (**C**) Retinal vertical section with blood vessels labeled by isolectin (*magenta*). Cholinergic amacrine cells, a source of acetylcholine, were immunolabeled for choline acetyltransferase (ChAT, *green*). Scale bar 40 µm. (**D**) Hypothesized cholinergic regulatory targets on pericytes and endothelial cells, leading to distinct capillary diameter changes. (**E**) Schematic presentation of established and proposed acetyl choline vasomotor actions. GCL, ganglion cell layer; INL, inner nuclear layer; IPL, inner plexiform layer; OPL, outer plexiform layer.

account for 84% of the total blood change during functional hyperemia.[12]

Multiple lines of evidence show that reduced blood supply in DR is linked to the deficit in cholinergic cells[13,14] making them both a significant factor in the DR pathophysiology and an attractive therapeutic target. However, the exogenous applications of ACh exerts a paradoxical vasoconstrictive action in retinal explants and isolated blood vessels.[7,9] This could be due to lack of both circuit specificity and spatial precision during pharmacological treatment as well as the choice of the model. Among available models, we focused on a well-established streptozotocin (STZ)-induced mouse model of DR.[15] This model could be easily induced without genetic manipulations, allowing precise timing of DR onset. Within 2 to 3 months after induction it has no vascular leakage, pericyte drop out, or acellular capillaries.[15–18] In this early stage of DR, no significant loss of ganglion cells was detected.[15,19] In the later stages of this model (6 months after STZ induction), acellular capillaries, vascular cell apoptosis, and formation of pericyte ghosts were detected.[15,20] In contrast to delayed anatomic changes, 4 weeks after STZ injection blood flow was reduced[21] and impairments in vasomotor responses were evident after 2 to 3 months.[16] Thus, this mouse model of early DR allows timely separation of early blood flow changes from later vascular and neuronal complications. Here, in an STZ mouse model of diabetes, we combined a targeted activation of cholinergic cells by genetic expression of Channelrhodopsin-2 (ChR2) with an in vivo assessment of capillary blood flow using two-photon imaging to test the hypothesis that selective light-driven stimulation of ACh released by its natural source - cholinergic amacrine cells - will promote a vasodilatory response and rescue capillary blood flow impairment in DR.

Methods

In all experimental procedures, animals were treated according to the regulations in the ARVO Statement for the Use of Animals in Ophthalmic and Vision Research, in compliance with protocols approved by the Institutional Animal Care and Use Committee (IACUC) of Weill Cornell Medicine (WCM), and in accordance with the National Institutes of Health Guide for the Care and Use of Laboratory Animals. The use and application of STZ were in accordance with safety protocols approved by Weill Cornell Medicine's Environmental Health and Safety, Institutional Biosafety Committee, and Institutional Animal Care and Use Committee Protection and Control subcommittee.

Experimental Animals

We generated a choline acetyltransferase promoter (ChAT)-ChR2 mouse line in which a light-sensitive ion channel, ChR2, is genetically expressed in all cholinergic amacrine

Investigative Ophthalmology & Visual Science

Table. Body Weight and Glucose Measurements in Experimental Animals

	1 D Before Injection		5 Wk After Injection		16 Wk After Injection	
Group	Weight, g	Glucose mg/dL	Weight, g	Glucose mg/dL	Weight, g	Glucose mg/dL
Nondiabetic wt (6 mice)	19.9 ± 0.4	176 ± 14	25.1 ± 0.7	167 ± 13	30.9 ± 1.0	156 ± 24
Nondiabetic ChAT-ChR2 (8 mice)	20.0 ± 0.9	163 ± 11	26.0 ± 0.7	178 ± 13	30.8 ± 1.0	167 ± 18
Diabetic wt (6 mice)	22.8 ± 1.6	175 ± 9	24.2 ± 1.6	383 ± 107	26.8 ± 2.8	349 ± 77
Diabetic ChAT-ChR2 (8 mice)	21.9 ± 1.8	178 ± 10	24.9 ± 1.8	345 ± 49	27.8 ± 1.7	300 ± 36
ANOVA	$P = 0.001$	$P = 0.059$	$P = 0.043$	$P < 0.0001$	$P < 0.0001$	$P = 0.0003$
Age	7 wk		12 wk		24 wk	

*Number in parenthesis indicates number of animals in each group.

cells, under the ChAT. To create the ChAT-ChR2 mouse line, we crossed homozygous ChAT-Cre mice (The Jackson Laboratory, B6; 129S6-Chattm2(cre)Lowl/J, stock #006410) with ChR2-YFP homozygous reporter mice (The Jackson Laboratory, B6;129S-Gt(ROSA)26Sortm32(CAG-COP4*H134R/EYFP)Hze/J, stock #012569). ChR2-YFP reporter is a lox-stop-lox line carrying LoxP sites flanking the STOP cassette that is deleted upon Cre recombination resulting in ChR2-YFP expression specifically in ChAT-Cre expressing cells. Both lines were originally created on a mixed C57BL/6;129 background. Upon arrival to Jackson Laboratory, these mice were bred to C57BL/6 mice to rederive their living colony. Thus, currently, both lines have C57BL/6 background, therefore, C57BL/6 mice were used as control animals. Diabetes was induced in two mouse lines: C57BL/6 mice (Jackson Laboratory, stock # 000664, RRID:IMSR_JAX:000664) and our ChAT-ChR2 mice. We used the STZ diabetic mouse.[15] Male mice aged 6 to 8 weeks were fasted for 4 hours prior to the injections. The animals were injected intraperitoneally on 5 consecutive days with 50 mg/kg STZ (Sigma-Aldrich, S0130) freshly dissolved in a citrate buffer (pH 4.5). Control animals received a citrate buffer injection without STZ. In our STZ mouse model of diabetes, the levels of blood glucose reached maximum elevation at 1 month after STZ injection and remained elevated. The diabetes was defined by nonfasting blood glucose greater than 250 mg/dL verified 1 month after the last STZ injection and confirmed on the day of the experiment. For recordings, diabetic animals were used 2 to 3 months after the last STZ-injection and their glucose was consistently above 250 mg/dL. A table of blood glucose and body weight of diabetic and nondiabetic mice is included (Table).

Two-Photon Recordings of Retinal Capillary Blood Flow

For the blood flow assessment in vivo, tail vein injection of 200 µl Sulforhodamine 101 (SR101, 10 mM; Sigma, #S7635) was performed 10 minutes prior to anesthesia. Each animal was initially anesthetized with a mixture of 75 mg/kg ketamine and 7.5 mg/kg xylazine. As the imaging procedure itself is not painful and we lost a few diabetic mice anesthetized with a full dose of anesthesia, we decided to decrease the anesthesia to half of the recommended surgical dose (surgical dose: 150 mg/kg ketamine and 15 mg/kg xylazine). This was sufficient for stable experiments, with all animals tolerating it well. The pupils were dilated with a 0.5% tropicamide ophthalmic solution, and a coverslip was placed on each eye with GONAK ophthalmic solution. Mice were mounted with a SG-4N mouse head holder (Narishige) on an upright ThorLabs Bergamo II two-photon microscope. During recordings, mice were placed on a heat pad and covered with a blanket, to maintain physiological temperature. Typically, capillary in nondiabetic wild type (wt) animals could be imaged immediately (12–15 minutes after single SR101 injection). This time point reflects maximum fluorescence in the capillaries. Capillaries in diabetic mice could be imaged at around 25 to 35 minutes, often after the second dose of SR101. Blood flow was measured using a 10 × super apochromatic objective with a 7.77 mm working distance and 0.5 NA (TL10X-2P; ThorLabs, Newton, NJ, USA). Using a long working distance, we first placed the objective as close to the eye as possible with the focus beyond the retina and without any fluorescent illumination. The focus was achieved in two-photon mode by moving the objective away from the eye. SR101 was illuminated with a 920 nm wavelength and the measurements were taken at a rate of 116 to 400 frames per second, depending on the size of the area of interest. At first, baseline blood flow in control nondiabetic and STZ-treated mice was recorded for 30 seconds. During this time, superficial, intermediate and deep capillary layers were measured by manually focusing through the retina; each layer was recorded for several seconds. Following baseline recordings, the eye was illuminated for 40 seconds through the same objective using a 480 nm blue LED flickering at 5 hertz (Hz). The optical separation between 488 nm ChR2 excitation and the 600 nm SR101 emission allowed simultaneous two-photon measurements while illuminating with the LED. At the end of light stimulation, each vascular layer was recorded for a total of 30 seconds. The time-lapse images were corrected for background, filtered with a Gaussian filter, and, when necessary, stabilized in Fiji (National Institutes of Health [NIH]). A stabilization plugin was used to eliminate strong movements of capillaries during deep animal breathing. Blood flow was estimated as the number of blood cells passing through a capillary per second. This analysis was performed in Fiji by plotting fluorescence profiles across blood vessels for every frame. In the resulting plot, troughs indicate the passage of a blood cell, which was darker relative to the plasma labeled with SR101. The peaks were automatically detected in Microsoft Excel and verified by visual inspection of the original data.[22]

Wholemount Retina Preparation for In Vitro Recordings

After euthanasia, both eyes were enucleated and placed in bicarbonate-buffered Ames solution, constantly equilibrated with 95% O_2 and 5% CO_2. All our measurements have been made under consistent O_2 levels across all exper-

Investigative Ophthalmology & Visual Science

imental conditions. For the retina wholemount preparation, the cornea, iris, and lens were removed and the retina was dissected into four equal quadrants.[23] Quadrants were placed on the photoreceptor surface down on a modified Biopore Millicell filter (Millipore, Burlington, MA, USA). This preparation was transferred to a recording chamber on the stage of an upright Nikon FN1 microscope equipped with Hoffman modulation contrast optics and bathed (1 mL/min) with bicarbonate-buffered Ames solution (A1420; Sigma, St. Louis, MO, USA). The following pharmacological agents were added to the Ames solution to block photoreceptor input to cholinergic cells: iGluR antagonist, 6-cyano-7-nitroquinoxaline-2,3-dione (CNQX, #C127, 10 uM; Sigma) and mGluR6 antagonist, L-(+)-2-amino-4-phosphonobutyric acid (L-AP4, #A212, 20 uM; Sigma). All experiments were performed at a near physiological temperature of 32 deg Celsius (°C). Whole-cell recordings were made from GFP labeled ChAT-ChR2 expressing cells using patch pipettes filled with an intracellular solution containing (in mM): 106 Cs-gluconate, 14 CsCl, 15 TEA-Cl, 1.0 CaCl2, 1.0 MgCl2, 11 EGTA, and 10 Na-HEPES, adjusted to pH 7.2 with cesium hydroxide. Electrodes were pulled from borosilicate glass (1B150F-4; WPI, Sarasota, FL, USA) using a P-97 Flaming/Brown puller (Sutter Instruments, Novato, CA, USA) and had a measured resistance of approximately 4 to 7 MΩ. All recordings were obtained using a MultiClamp 700B patch-clamp amplifier (Molecular Devices, Sunnyvale, CA, USA). Data were filtered at 5 kHz with a four-pole Bessel filter and were sampled at 15 kHz.

Light Stimulation

To activate channelrhodopsin of ChAT-ChR2 cells in living retinal explants, the microscope's illuminator was used to deliver a 200 µm spot of light centered on the inner retina. An aperture, a series of neutral density filters, the FN-C LWD condenser (Nikon), and a Uniblitz shutter (Vincent Associates) were used to control the size, intensity, focal plane, and duration of the stimulus, respectively. Stimulation routines were controlled by Signal 2 software (CED). The tissue was light adapted at 30 cd/m2. The intensity of the light stimuli was changed in steps of either 0.25 or 0.5 log units, ranging from 10 to 10,000 Rh*/rod/s above adapting level, covering the range of cone-mediated responses.

Antibodies and Other Reagents

Two antibodies to cholinergic cells were used: anti choline acetyltransferase (ChAT, goat polyclonal, Millipore Cat # AB144P, RRID:AB_2079751, 1:2000) and anti-vesicular ACh transporter (VAChT, rabbit polyclonal, Alomone Labs Cat # ACT-003, RRID:AB_2340929, 1:2000). The anti-ChAT antibody labels the cytoplasm of cholinergic cells including the soma and fine processes, whereas anti-VAChT labels the synapses of cholinergic cells. Blood vessels were visualized by labeling with isolectin. Griffonia simplicifolia isolectin conjugated to a fluorescent label were acquired from Invitrogen (GS-IB4 Alexa Fluor 568, I21412). The isolectin stock solution was made using 500 µg of isolectin powder dissolved in 500 µL of phosphate-buffered saline (PBS)-calcium solution containing (in mM): 8.1 Na2HPO4 dibasic, 1.9 NaH2PO4 monobasic, 154 NaCl, and 1 mM CaCl2. Isolectin stock solution was diluted 1:400 and applied with the secondary antibodies that were conjugated to Alexa 568 (1:1000; red fluorescence; Molecular Probes), or Cy3 (1:1000; red fluorescence; Jackson ImmunoResearch).

Immunohistochemistry

After in vivo blood flow recordings, the animals were euthanized, and the eyes were removed and placed in bicarbonate-buffered Ames' medium (Sigma Aldrich, St Louis, MO, USA) equilibrated with 95% O_2 and 5% CO_2. The cornea was removed by an encircling cut above the ora serrata, then the iris, lens, and vitreous were extracted. The remaining eyecup, with the retina still attached to the pigment epithelium, was submersion-fixed on a shaker with freshly prepared 4% paraformaldehyde in 0.1 M PBS (pH = 7.3), for 15 minutes at room temperature. After fixation, the eye cups were washed in PBS for 2 hours. Retinal eyecup preparations were blocked for 10 hours in a PBS solution containing 5% Chemiblocker (membrane-blocking agent; Chemicon), 0.5% Triton X-100, and 0.05% sodium azide (Sigma). Primary antibodies were diluted in the same solution and applied for 96 hours, followed by incubation for 48 hours in the appropriate secondary antibody. In multilabeling experiments, eye cup preparations were incubated in a mixture of primary antibodies, followed by a mixture of secondary antibodies. All steps were completed at room temperature. After staining, the tissue was flat-mounted on a slide, ganglion cell layer up, and coverslipped using Vectashield mounting medium (H-1000; Vector Laboratories). The coverslip was sealed in place with nail polish. To avoid extensive squeezing and damage to the retina, small pieces of a broken glass cover slip (number 1 size) were placed in the space between the slide and the coverslip. Retinal wholemounts were imaged on a Leica SP8 confocal microscope using 20 x air and 63 x oil objectives.

Statistical Analysis

Statistical analysis was performed in Excel using the *t*-test function for two-group comparisons. The data are presented as mean ± standard deviation (SD). To avoid introducing nonindependent data into statistical analysis, first, multiple samples from individual animals were averaged within each subject, then the data between animals were compared.[24]

Results

Capillary Blood Flow is Impaired Along all Retinal Vascular Layers in Early Stages of DR

Reduced capillary blood flow is the earliest diagnostic hallmark of patients with DR. However, the majority of studies of diabetes in animal models focus primarily on later stages of the disease, with manifest changes to vascular structures and the blood retina barrier (BRB). Therefore, in our animal model of diabetes, we first wanted to establish the prevalence of capillary blood flow changes in early DR. In male mice injected with STZ, a common model of type 1 diabetes, and age-matched sham controls, we measured capillary blood flow 2 to 3 months after the last treatment. As we previously reported, no signs of anatomic changes to capillaries or BRB integrity were evident at this early stage.[16] To prevent morbidity of sensitive diabetic mice, a light anesthesia was induced by administering half of the recommended dose of anesthetic in all recorded groups (see Methods). A high-speed two-photon imaging system (Thor-

Investigative Ophthalmology & Visual Science

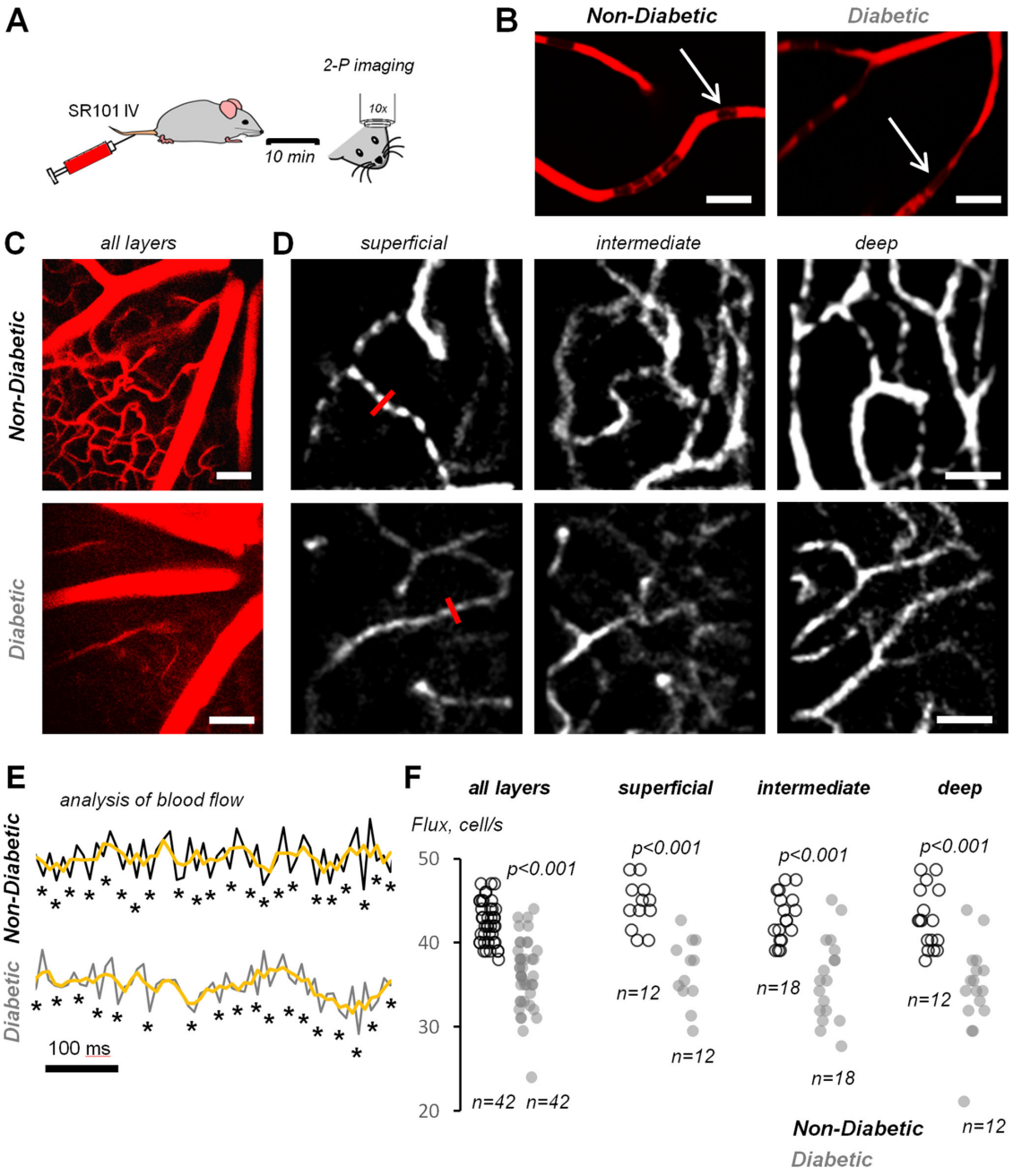

Figure 2. Retina capillary blood flow impairment during early stages of diabetic retinopathy. (**A**) Experimental paradigm of two-photon imaging of retinal capillary blood flow in mice after tail vein infusion of sulforhodamine 101 (SR101). (**B**) After IV injection, SR101 is fully contained in the blood vessel lumen as shown in a high magnification image of an isolated retinal wholemount from nondiabetic and diabetic mice. No endothelial cells or pericytes were labeled. *Arrow* shows a blood cell inside the lumen. Scale bar 10 mm. (**C**) In vivo, following SR101 injection, the retinal arteries were well infused with SR101 in both nondiabetic and diabetic mice. The intensity of SR101 in capillaries of diabetic retina was less than in nondiabetic controls, indicative of reduces perfusion rate. Scale bar 25 mm. (**D**) By focusing through the retina, each vascular layer could be identified and assessed separately. *Red lines* show examples of capillary crossings where blood flow was measured. (**E**) Profiles through a time-lapse image of a capillary marked by red lines in **D**. *Yellow lines* indicate moving averages. All peaks below the *yellow lines* were counted. (**F**) Basal blood flow, counted as number of peaks per second in **E**, in capillaries of nondiabetic mice was significantly higher than in diabetic littermates. Six diabetic and six nondiabetic mice; N = total number of samples; t-test was used for comparison.

Labs), equipped with a long-distance 10 x objective was used to monitor capillary blood flow across all retinal vascular layers. To visualize retinal vasculature and to enhance the discrimination of blood cell movement within the capillaries, a fluorescent contrast agent Sulforhodamine 101 (SR101) was injected into the tail vein (Fig. 2A). In our extensive testing of various contrasting reagents, such as fluorescein, Evans Blue, or Sulforhodamine B, we found that the use of SR101 was advantageous for the following reasons.[22] First, in our working application (see Methods), SR101 displayed

Investigative Ophthalmology & Visual Science

minimal toxicity. This is in contrast to Evans Blue, which was not well-tolerated by the animals. Second, SR101 remained inside blood vessels of both nondiabetic and diabetic retinas and was not released into surrounding tissue (Fig. 2B). Third, in two-photon microscopy SR101's excitation peak is > 920 nm, which is red-shifted in relation to fluorescein (800 nm) and sulphorhodamineB (< 900 nm) and away from visible light. Fourth, it exhibits a high signal-to-noise ratio, thus requiring reduced laser power.

In our experiments, capillaries in nondiabetic wt animals could be imaged 12 to 15 minutes after single SR101 injection. In contrast, at 15 minutes following a single dose of SR101, fluorescence levels were not sufficient for imaging capillary blood flow in diabetic animals. Capillaries in diabetic mice could be imaged at around 25 to 35 minutes, often after a second dose of SR101. The poor filling of capillaries in diabetic retinas is likely because of their constriction (Fig. 2B; compared with the shape of the red blood cells in nondiabetic and diabetic retina). In contrast to capillaries, large vessels appeared to be well-filled in diabetic mice (Fig. 2C).

To quantify blood flow, we imaged each vascular layer for approximately 10 seconds at a rate of 116 frames per second to directly monitor the rate of blood cells crossing an imaginary capillary region (Fig. 2D and Methods). To account for heartbeat fluctuations during in vivo imaging, blood cell crossing events were discriminated using a running average threshold routine (Fig. 2E; Methods). This approach allowed for a robust and direct assessment allowing the comparison of capillary blood flow across individual vascular layers in the living mouse eye. Using this protocol, we found that 2 to 3 months post STZ treatment the basal capillary blood flow was significantly reduced in diabetic mice compared with nondiabetic sham treated controls (nondiabetic, 6 mice, 42 samples: 43 ± 2 cell/s; diabetic, 6 mice, 42 samples: 36 ± 4 cell/s; *t*-test, $P < 0.001$; Fig. 2F). Notably, this capillary blood flow reduction was evident at superficial (nondiabetic, 6 mice, 12 samples: 44 ± 2 cell/s; diabetic, 6 mice, 12 samples: 36 ± 3 cell/s; *t*-test, $P < 0.001$), intermediate (nondiabetic, 6 mice, 18 samples: 42 ± 2 cell/s; diabetic, 6 mice, 18 samples: 36 ± 4 cell/s; *t*-test, $P < 0.001$), and deep (nondiabetic, 6 mice, 12 samples: 42 ± 3 cell/s; diabetic, 6 mice, 12 samples: 35 ± 5 cell/s; *t*-test, $P < 0.001$) vascular layers. In addition to an overall reduction in resting circulation, diabetic mice also exhibited capillaries with an apparent stalled blood flow. These unusually slow capillaries were detected across all vascular layers.

Selective Optogenetic Stimulation of Cholinergic Amacrine Cells Dilates Retinal Vasculature

Because the retina lacks central vascular innervation, local retinal circuits regulate proximal blood flow. Among numerous vasoactive neurotransmitters, ACh is of particular interest as it is a potent physiological vasomodulator that is released by a genetically defined class of cholinergic amacrine cells. Their target, m3AChRs have been shown to be expressed by both vascular endothelial and mural cells, including pericytes,[6,9,10] with potentially diverging outcomes to capillary diameter and blood flow. Therefore, in our study, we tested the hypothesis that in vivo cell-targeted stimulation of ACh release by its native source (cholinergic amacrine cells) will restore a physiological vasodilatory response and rescue capillary blood flow impairment in early diabetes (Fig. 3). For this purpose, we generated a mouse line in which a light-sensitive cation channel, ChR2, is genetically expressed in all cholinergic amacrine cells, under the ChAT (Fig. 3A). Utilizing the Cre/LoxP system, we crossed homozygous ChAT-Cre mice with a ChR2-YFP reporter mouse. ChR2-YFP reporter is a lox-stop-lox line carrying LoxP sites flanking the STOP cassette that is deleted upon Cre recombination resulting in ChR2-YFP expression in ChAT-Cre positive cells. In our experiments, we used heterozygous ChAT-ChR2-YFP animals. In these mice, ChR2-YFP expression overlapped 100% with ChAT immunoreactivity, suggesting that all cholinergic cells, and only cholinergic cells, express the construct (Figs. 3B, 3C). Nondiabetic wt and ChAT-ChR2 retinas had similar anatomy and distribution of cholinergic cells. ChR2 is a transmembrane ion channel, and, indeed, its expression was localized to the membrane of the cholinergic cells, unlike ChAT, which was evenly distributed in the cytoplasm of cholinergic amacrine cells (see Figs. 3B, 3C). Therefore, ChAT-labeled cells may appear to be smaller than ChR2-YFP visualized cholinergic cells. No real change in size was detected. ChR2 was also expressed by processes of both ON- and OFF-cholinergic amacrine cells. Importantly, there was a robust innervation and ChR2 expression along the capillaries within the sublaminar vascular layer, the site of direct cholinergic interactions with the microvasculature on its supply route to intermediate and deep vascular layers.[3] The vasculature of wt and ChAT-ChR2 retinas had similar appearance (Fig. 3D).

Next, we wanted to confirm that the expression of ChR2 was sufficient to activate cholinergic amacrine cells. For this, we performed single cell patch-clamp recordings by targeting ChR2-GFP-positive cells in freshly dissected nondiabetic retinal wholemounts. To confirm that the targeted cell was indeed a cholinergic amacrine cell, it was backfilled with Alexa 568, and included in the patch-pipette solution (see Fig. 3C, insert). Indeed, the recorded ChR2-positive cell exhibited a characteristic starburst dendritic morphology (Fig. 3E) and was further identified by ChAT immunolabeling (see Fig. 3C). ChR2-induced activity was induced by light, in the presence of synaptic blockers (L-AP4, 50 uM, and CNQX, 5 uM) to block photoreceptor driven inputs. Membrane potential recordings from cholinergic amacrine cells in ChAT-ChR2-YFP mice showed an activation threshold and temporal activity profiles consistent with a ChR2-driven response.[25] Next, we confirmed that selective stimulation of cholinergic cells with ChR2-induced depolarization would indeed trigger a vasomotor response comparable to agonist-driven cholinergic activation. Consistently with this, ChR2-assisted light activation of cholinergic amacrine cells produced a modest dilation of both capillaries and precapillary regions (Figs. 3G, 3H; 7.28 ± 3.87% increase over baseline $P = 0.03$, and 10.87 ± 3.96% increase over the baseline, $P = 0.01$, *t*-test, respectively. N = 15 each group).

In Vivo Optogenetic Stimulation of Cholinergic Amacrine Cells Improves Basal Level of Capillary Blood Flow in DR

After successful functional expression of ChR2 in cholinergic cells, we measured basal blood flow in retinal capillaries of nondiabetic and diabetic ChAT-ChR2 mice, filled with SR101 (Figs. 4A, 4B). Blood vessel shapes and permeability to SR101 was not affected by the presence of ChR2 in cholinergic cells. Both ON- and OFF-cholinergic cells were present

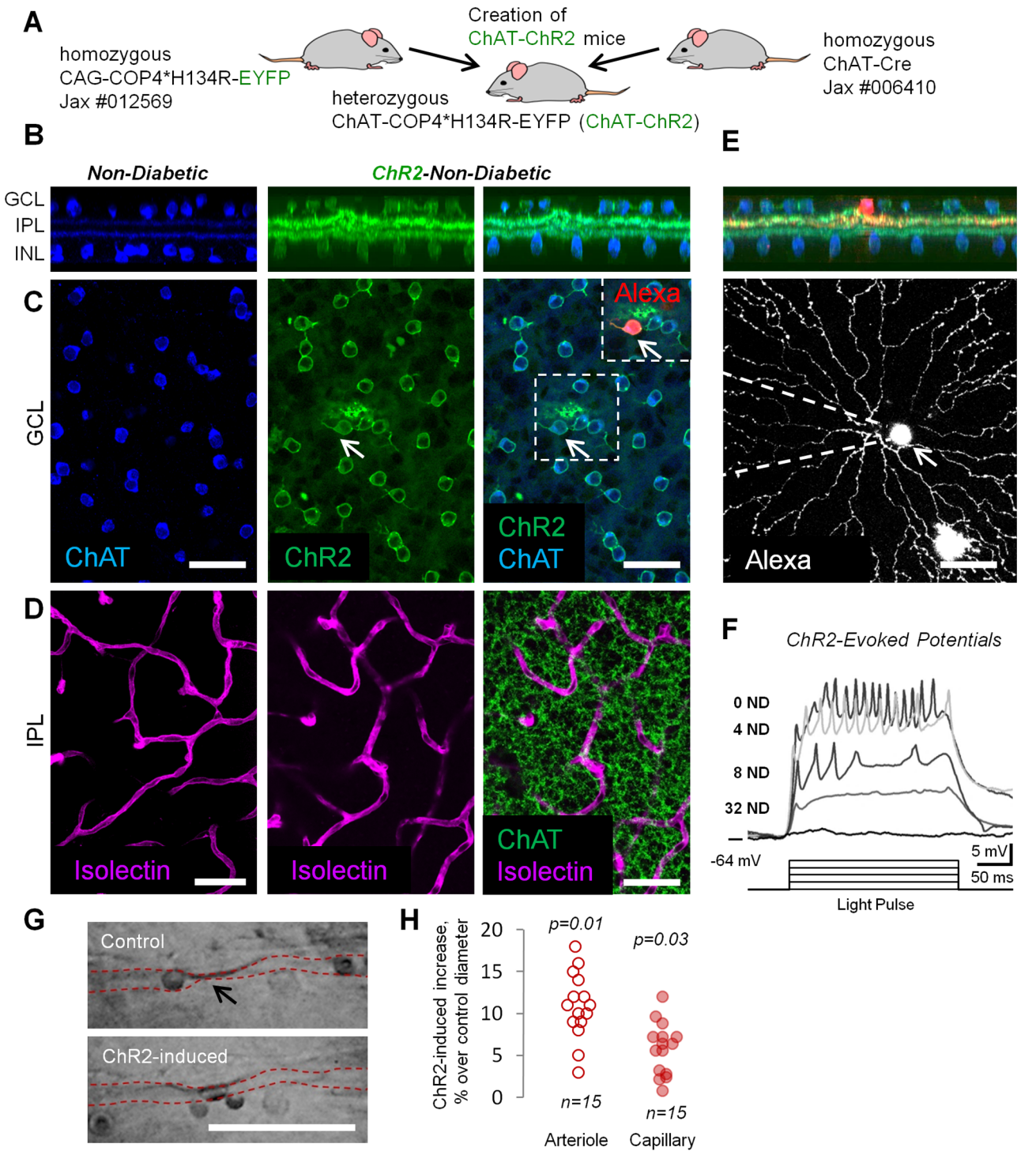

Figure 3. Channelrhodopsin-2 (ChR2) assisted probing of the cholinergic pathways in nondiabetic retina. (**A**) Creation of ChAT-ChR2 heterozygous mice. (**B**) Confocal images in *wt* and ChAT-ChR2-YFP retinal wholemounts stained for ChAT (*blue*). In ChAT-ChR2-YFP, a robust expression of ChR2 retina is visualized by YFP fluorescence (*green*). In this mouse, both ON and OFF ChAT-positive cells (*blue*) contain ChR2. (**C**) In the same retinal ChAT-ChR2 wholemount shown in **B**, the GFP-positive ChR2-expressing cell was targeted for electrophysiological recordings and backfilled with Alexa 568 included in recording pipette (*arrow*, *red*). Scale bar 50 µm. (**D**) Blood vessels were similar in wt and ChAT-ChR2-YFP retinas. The site of potential interaction of ChR2-positive cholinergic cells (*green*) and blood vessels (*magenta*) is located in the IPL. (**E**) Note a characteristic starburst appearance of the filled ChAT-positive amacrine cell from **B**. (**F**) Spiking activity in current-clamp mode from the cell in **E** in presence of synaptic blockers (LAP4 and NBQX). Flashing pots of light of varying intensity produced characteristic sustained and non-desensitizing ChR2-driven membrane depolarization. ND values represent the neutral density filter attenuation of light from the light source. (**G**) ChR2-assisted light activation of cholinergic amacrine cells produces dilation of capillaries and pre-capillary arterioles. Vasomotor response was measured when photoreceptor inputs were blocked by a mixture of CNQX and L-AP4. *Arrowhead* points at region of dilation, allowing passage of a blood cell. Scale 30 µm. (**H**) Quantification of vasomotor response across arterioles and capillaries from **G**; N = total number of samples; paired t-test.

Investigative Ophthalmology & Visual Science

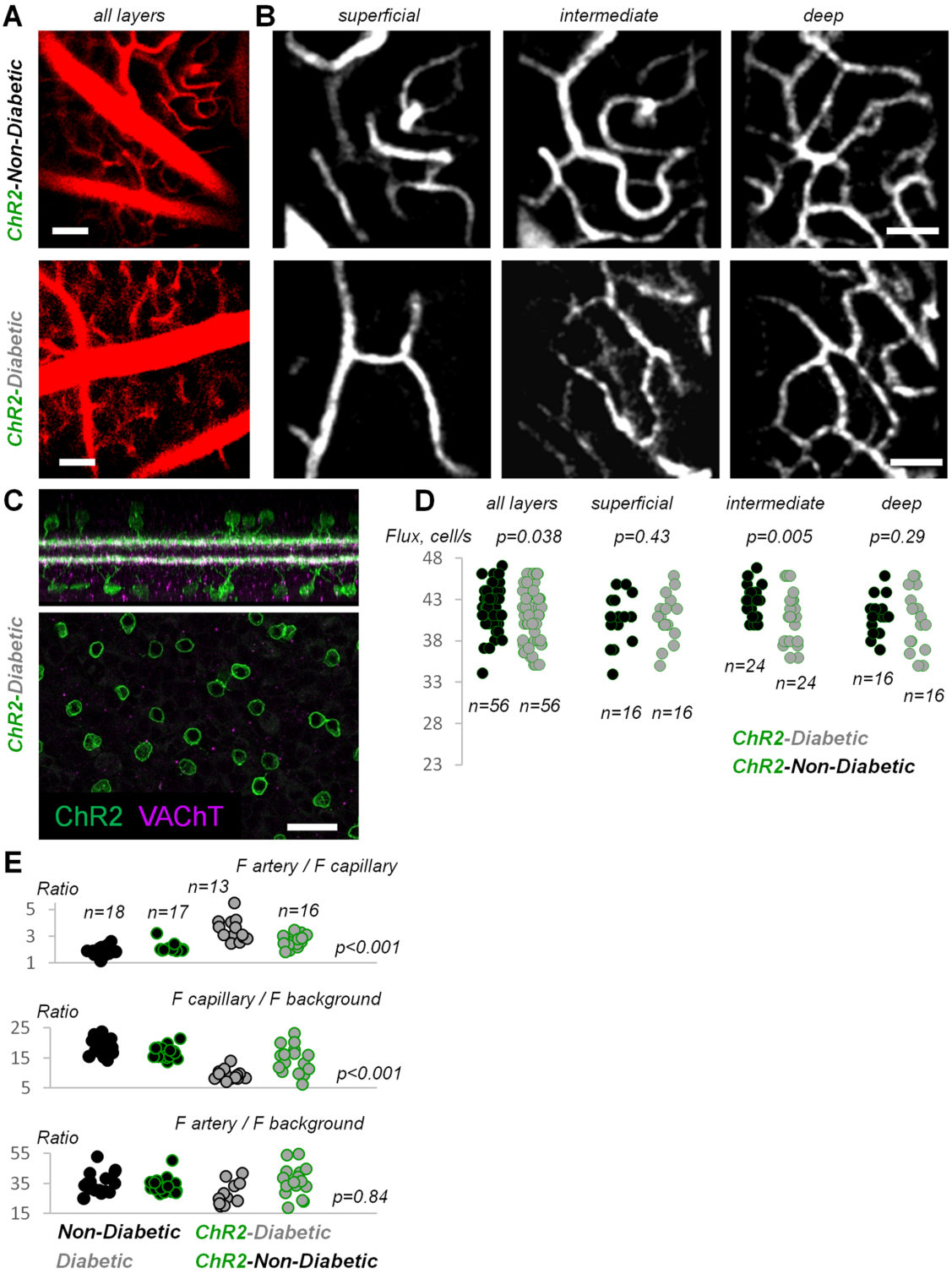

Figure 4. Basal retinal capillary blood flow is improved in ChAT-ChR2-diabetic animals. (**A**) Two-photon images of mouse retina after tail vein infusion of sulforhodamine 101 (SR101). Large vessels and capillaries are well-filled with SR101. Scale bars 25 mm. (**B**) Individual vascular layers where blood flow was recorded. Scale bars 25 mm. (**C**). After in vivo measurements, wholemount retinas of ChAT-ChR2-diabetic animals were processed to assess ChR2 (*green*) and vesicular acetyl choline transporter (VAChT, *magenta*) labeling. (**D**) Quantification of basal blood flow in capillaries of ChR2-diabetic and ChR2-nondiabetic mice. Eight diabetic and eight nondiabetic mice Chat-ChR2 mice; *N* indicates total number of samples; *t*-test was used for comparison. (**E**) Filling of the retinal capillary with SR101 was significantly different in diabetic mice, as reflected by the different artery to capillary and capillary to background ratios. In contrast, the ratio between artery and background was similar for all lines. *N* = total number of samples; ANOVA was used for comparison.

Investigative Ophthalmology & Visual Science

in diabetic ChAT-ChR2 mice, and ChR2 was expressed at their membranes, including soma and processes (Fig. 4C, green). Moreover, normal synaptic distribution of vesicular ACh transporter was observed in all cholinergic cells (see Fig. 4C, magenta). Although the basal capillary blood flow was statistically different between nondiabetic and diabetic ChAT-ChR2 mice (nondiabetic ChAT-ChR2, 8 mice, 56 samples: 42 ± 3 cell/s; diabetic ChAT-ChR2, 8 mice, 56 samples: 40 ± 3 cell/s; *t*-test, $P = 0.038$), the greatest difference was detected in the intermediate layer (nondiabetic ChAT-ChR2, 8 mice, 24 samples: 43 ± 2 cell/s; diabetic ChAT-ChR2, 8 mice, 24 samples: 41 ± 3 cell/s; *t*-test, $P = 0.005$). Blood flow in the superficial layer (nondiabetic ChAT-ChR2, 8 mice, 16 samples: 41 ± 3 cell/s; diabetic ChAT-ChR2, 8 mice, 16 samples: 41 ± 3 cell/s; *t*-test, $P = 0.43$) and deep layer (nondiabetic ChAT-ChR2, 8 mice, 16 samples: 41 ± 2 cell/s; diabetic ChAT-ChR2, 8 mice, 16 samples: 40 ± 4 cell/s; *t*-test, $P = 0.41$) was comparable.

Next, we compared basal blood flow in diabetic wt (see Fig. 2) and diabetic ChAT-ChR2 mice (see Fig. 4). Blood flow was significantly increased in all capillary layers of ChAT-ChR2 mice: superficial layer (diabetic wt, 6 mice, 12 samples: 36 ± 3 cell/s; diabetic ChAT-ChR2, 8 mice, 16 samples: 41 ± 3 cell/s; *t*-test, $P = 0.001$), intermediate (diabetic wt, 6 mice, 18 samples: 36 ± 4 cell/s; diabetic ChAT-ChR2, 8 mice, 24 samples: 41 ± 3 cell/s; *t*-test, $P < 0.001$), and deep layer (diabetic wt, 6 mice, 12 samples: 35 ± 5 cell/s; diabetic ChAT-ChR2, 8 mice, 16 samples: 40 ± 4 cell/s; *t*-test, $P = 0.0035$). In line with increased blood flow in diabetic ChAT-ChR2 mice, their capillaries were also better filled with SR101 as reflected by artery to capillary gradient (nondiabetic wt, 6 mice, 18 samples: 1.88 ± 0.33; diabetic wt, 6 mice, 13 samples: 3.43 ± 0.83; nondiabetic ChAT-ChR2, 8 mice, 17 samples: 2.07 ± 0.30; diabetic ChAT-ChR2, 8 mice, 16 samples: 2.59 ± 0.46; ANOVA, $P < 0.001$) and capillary to background ratio (nondiabetic wt, 6 mice, 18 samples: 18.7 ± 2.9; diabetic wt, 6 mice, 13 samples: 9.4 ± 1.7; nondiabetic ChAT-ChR2, 8 mice, 17 samples: 16.8 ± 2.0; diabetic ChAT-ChR2, 8 mice, 16 samples: 14.4 ± 4.5; ANOVA, $P < 0.001$; Fig. 4E). As a result, diabetic mice with ChR2 had faster filling of the capillaries (18–25 minutes) than diabetic mice without ChR2 (25–35 minutes). We did not see any significant leakage of SR101 from capillaries in any mouse line that is supported by a similar artery to background ratios (nondiabetic wt, 6 mice, 18 samples: 35 ± 7; diabetic wt, 6 mice, 13 samples: 33 ± 13; nondiabetic ChAT-ChR2, 8 mice, 17 samples: 35 ± 7; diabetic ChAT-ChR2, 8 mice, 16 samples: 36 ± 10; ANOVA, $P = 0.84$).

Basal increase in capillary blood flow in diabetic ChAT-ChR2 mice suggests that ACh release is important for regulating the basal tone of the capillaries because ChR2 was likely active during the routine animal daylight activity preceding blood flow measurements.

Optogenetic Boost of Cholinergic Cells did not Rescue Functional Hyperemia in ChAT-ChR2 Diabetic Mice

Finally, we compared light-induced blood flow changes in all four groups of mice. The animals were injected with SR101 and, after recording of basal blood flow in all vascular layers, were stimulated with a 30 second long 5Hz flickering blue light (480 nm; Fig. 5A). This light exposure was estimated to be sufficient to directly stimulate both photoreceptors and ChR2 in cholinergic cells of ChAT-ChR2 mice. Indeed, in nondiabetic wt mice, a significant increase in blood flow was induced in the superficial (nondiabetic, 6 mice, 12 samples: basal 44 ± 2 cell/s and after stimulation 47 ± 2 cell/s; paired *t*-test, $P < 0.001$) and deep (nondiabetic, 6 mice, 12 samples: basal 44 ± 3 cell/s and after stimulation 47 ± 2 cell/s; paired *t*-test, $P < 0.001$) vascular layers. However, whereas the majority of capillaries in the intermediate vascular layer displayed an increased blood flow, only few capillaries had a reduction in their blood flow, thus eliminating the statistical significance of the change (nondiabetic, 6 mice, 12 samples: basal 42 ± 2 cell/s and after stimulation 44 ± 3 cell/s; paired *t*-test, $P = 0.13$; 50% capillaries increased blood flow). This bidirectional change of blood flow in response to the ChR2-activating light may be a physiological way to redistribute blood flow between the layers based on the neuronal demand. Similar trends were observed in nondiabetic ChAT-ChR2 mice in the superficial (nondiabetic ChAT-ChR2, 8 mice, 16 samples: basal 41 ± 3 cell/s and after stimulation 45 ± 4 cell/s; paired *t*-test, $P < 0.001$), intermediate (nondiabetic ChAT-ChR2, 8 mice, 24 samples: basal 43 ± 2 cell/s and after stimulation 42 ± 4 cell/s; paired *t*-test, $P = 0.08$; 33% capillaries increased blood flow), and deep (nondiabetic ChAT-ChR2, 8 mice, 16 samples: basal 41 ± 2 cell/s and after stimulation 45 ± 2 cell/s; paired *t*-test, $P < 0.001$) vascular layers. In contrast, no functional hyperemia was evident in diabetic nontransgenic mice with no detectable blood flow changes in the superficial (diabetic, 6 mice, 12 samples: basal 36 ± 3 cell/s and after stimulation 37 ± 3 cell/s; paired *t*-test, $P = 0.3$), intermediate (diabetic, 6 mice, 18 samples: 36 ± 4 cell/s; and after stimulation 36 ± 4 cell/s; paired *t*-test, $P = 0.4$), and deep (diabetic, 6 mice, 18 samples: 35 ± 5 cell/s; and after stimulation 36 ± 6 cell/s; paired *t*-test, $P = 0.3$) vascular layers. In diabetic ChAT-ChR2 mice, little change in blood flow was detected in the superficial (diabetic ChAT-ChR2, 8 mice, 16 samples: 41 ± 3 cell/s; and after stimulation 42 ± 3 cell/s; paired *t*-test, $P = 0.023$) but not in the deep layer (diabetic ChAT-ChR2, 8 mice, 24 samples: 41 ± 4 cell/s; and after stimulation 36 ± 6 cell/s; paired *t*-test, $P = 0.4$). In the intermediate layer, blood flow did not change (diabetic ChAT-ChR2, 8 mice, 16 samples: 41 ± 3 cell/s; and after stimulation 41 ± 4 cell/s; paired *t*-test, $P = 0.42$).

Discussion

The retina is one of the most metabolically demanding organs in the human body; even small changes in blood supply may contribute to vision loss. The goal of this study was to test whether a gene-targeted optogenetic activation of a potent vasoactive system of cholinergic cells would rescue early capillary microcirculation disruption observed in DR. Below, we discuss our major findings, potential mechanisms, and their implications for the use of optogenetic approaches as therapeutic strategies for early DR.

Targeting Neurovascular Unit Interactions for Capillary Blood Flow Repair in DR

Here, we explored the efficacy of targeting a well-defined neuronal cell population to prevent capillary blood flow impairment, an early pathophysiological event in patients with diabetes. The neurovascular approach may be an effective therapeutic strategy for a number of reasons.

Investigative Ophthalmology & Visual Science

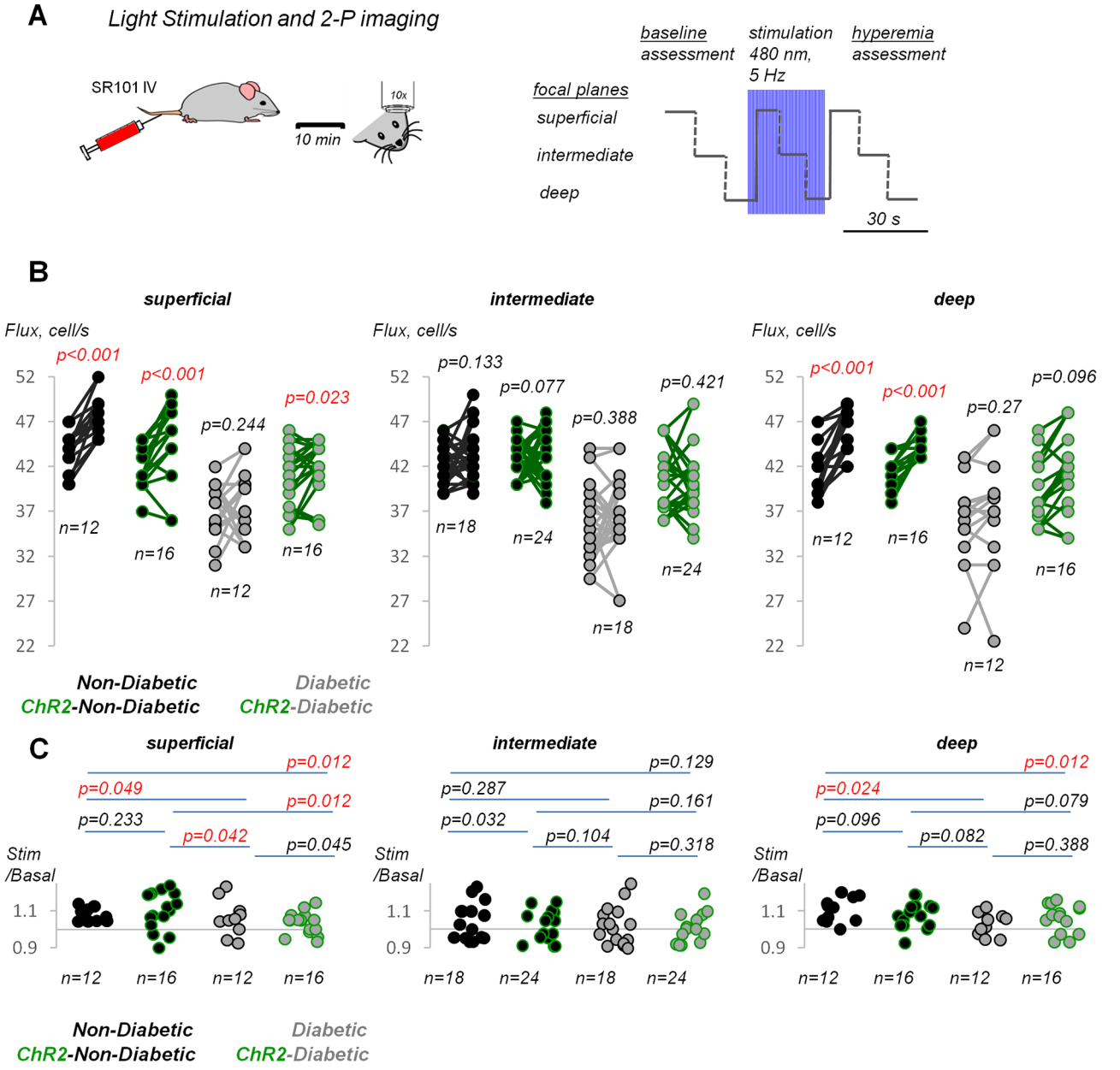

Figure 5. Functional hyperemia is not restored in the retinas of ChAT-ChR2-diabetic mice. (**A**) Protocol for assessment of baseline blood flow and functional hyperemia. (**B**) Changes of blood flow after stimulation with blue LED. Paired *t*-test. (**C**) Ratios of blood flow after stimulation to the baseline, *t*-test. *N* = total number of samples. Six diabetic and six nondiabetic wt mice; 8 diabetic and 8 nondiabetic mice ChAT-ChR2 mice.

First, because the disruption in retinal microcirculation far precedes more obvious changes to the vascular structure and BRB integrity, it provides a wide window of opportunity for intervention. Second, targeting pathophysiological processes at the onset of DR may lessen or prevent the progression of DR-induced degeneration. Third, a systems approach targeting neurons, vasculature, and glia during early events may prevent future complications in DR.

Due to high metabolic demand of brain tissue, the interactions within the neurovascular unit, an ensemble of neurons, and glia and vascular cells, have been increasingly recognized as key factors in early pathophysiology in a broad range of diseases.[26] In response to light stimulation, retinal cholinergic amacrine cells release acetylcholine that activates m3AChRs on vascular cells. However, the role of ACh on endothelial cells and pericytes remains controversial. Indeed, it has been suggested that the vasodilatory action of ACh is linked to its activation of muscarinic m3AChRs on endothelial cells, leading to NO synthesis and pericyte hyperpolarization and relaxation.[6] However, direct activation of m3AChRs on pericytes leads to their constriction.[8] In our optogenetic stimulation paradigm, activation of ACh release induced a significant vasodilatory response, resulting in an increase in basal capillary blood flow across retinal

Investigative Ophthalmology & Visual Science

vascular layers, suggesting that both circuit and site-specific ACh delivery may be required for the physiological dilatory action of ACh (also discussed below).

Our data demonstrate an improved blood flow in the superficial layer upon optogenetic stimulation, supporting an active role for ON ChAT cells in activating mACh receptors either on the superficial vasculature and/or diving capillaries. We cannot exclude that local activation of both OFF and ON ChAT cells may also affect blood flow in upstream precapillary regions and arteries by means of spreading vasoactive signals along the gap-junction-mediated vascular relay[27] (PMID: 30950036). Further dissection will require identification of ACh release and diffusion dynamics, which we are currently investigating in a separate study, by means of ACh fluorescent sensors.[28]

Optogenetics as a Strategy to Treat Blood Flow Impairment in DR

Since the expression of ectopic light-sensitive proteins for the treatment of photoreceptor degenerative diseases,[29] the use of optogenetics as a therapeutic strategy has seen an exponential growth in numerous retinal neuronal degenerative diseases.[30,31] This study provides the first line of evidence as to the applicability of optogenetic strategies in amplifying cholinergic signaling to treat a systemic microvascular disease, such as diabetes. Indeed, earlier studies of STZ-treated rats exhibited reduced cholinergic-dependent vasodilation within 2 to 6 week after the final STZ treatment.[13,14] This was concurrent with the onset of decreased microcirculation in both diabetic rats[32] and mice.[33] However, exogenous delivery of ACh has led to mixed outcomes in retinal explant or isolated blood vessel models, indicative of multiple signaling pathways in the cholinergic regulation of blood vessel physiology (Fig. 1E).[8,9] Not only do these models lack the comprehensive physiological support provided in vivo (blood pressure, temperature, and ischemia), but the outcome was assessed by much coarser metrics (e.g. BV diameter), than the capillary flow rate analyzed in the present study. Moreover, the high spatio-temporal resolution afforded by ChR2 in an organ (the eye) naturally designed to focus the actuator (light) in spatio-temporal coincidence to the region of natural-stimulus processing (thus most likely to require metabolic support) is far superior to bath application of ACh agonists.

Circuit specific strategies, such as optogenetic stimulation of a genetically defined cell population, may also help address another critical unanswered question in ACh action on blood flow - local versus volume transmission.[34] A recent direct visualization of the spread of released ACh in the hippocampus using the GACh sensor, a genetically encoded ACh metabotropic fluorescent reporter, helped estimate the spread constant of ACh transmission as within the range of 9 to 15 um.[28] In relation to retinal anatomy, this translates to a fraction of the IPL thickness, suggesting that ACh may act with cellular and/or subcellular specificity. Importantly, this also indicates that bath application of AChR modulators, a commonly used route of administration, may be less physiological than was previously understood. It is appealing, albeit not experimentally tested, that the lamina-specific regulation of blood flow is linked to the prevalence of BOLD functional magnetic resonance imaging (fMRI) signal at light flicker offset.[35] Thus, the optogenetic approach may prove advantageous to pharmacological application of AChR agonists as it utilizes a natural retinal stimulus: light. Indeed, optogenetic stimulation enables a tissue specific and spatially accurate delivery of ACh, which cannot be accomplished by any conventional pharmacological treatment strategies. The surprising outcome that ChR2 stimulation did not improve flicker-induced increase in blood flow may be due to a simultaneous dilation of both capillaries and arterioles, thus reducing blood pressure. In light of OFF- cholinergic cell processes densely innervating the sublaminar vascular plexus,[3] a potential solution would be to selectively target the ON- and OFF- cholinergic cell populations with opsins sensitive to different wavelengths. Future experiments aimed at discriminating the anatomic structures driving basal blood flow from functional hyperemia will prove particularly helpful. In conclusion, there is accumulating evidence that progression of DR involves changes to all components of the neurovascular unit - neurons, glia, vascular contractile cells, and endothelium.[1] The findings of this study provide direct support to the utility of an optogenetic approach to target distinct retinal circuits for treating DR and its complications.

Acknowledgments

Supported by NIH grants R01-EY026576 and R01-EY029796 (B.T.S.).

Disclosure: **E. Ivanova,** None; **P. Bianchimano,** None; **C. Corona,** None; **C.G. Eleftheriou,** None; **B.T. Sagdullaev,** None

References

1. Antonetti DA, Klein R, Gardner TW. Diabetic retinopathy. *N Engl J Med*. 2012;366:1227–1239.
2. Thebeau C, Zhang S, Kolesnikov AV, Kefalov VJ, Semenkovich CF, Rajagopal R. Light deprivation reduces the severity of experimental diabetic retinopathy. *Neurobiol Dis*. 2020;137:104754.
3. Ivanova E, Toychiev AH, Yee CW, Sagdullaev BT. Intersublaminar vascular plexus: the correlation of retinal blood vessels with functional sublaminae of the inner plexiform layer. *Invest Ophthalmol Vis Sci*. 2014;55:78–86.
4. Peppiatt CM, Howarth C, Mobbs P, Attwell D. Bidirectional control of CNS capillary diameter by pericytes. *Nature*. 2006;443:700–704.
5. Kornfield TE, Newman EA. Regulation of blood flow in the retinal trilaminar vascular network. *J Neurosci*. 2014;34:11504–11513.
6. Gericke A, Sniatecki JJ, Goloborodko E, et al. Identification of the muscarinic acetylcholine receptor subtype mediating cholinergic vasodilation in murine retinal arterioles. *Invest Ophthalmol Vis Sci*. 2011;52:7479–7484.
7. Benedito S, Prieto D, Nielsen PJ, Nyborg NC. Role of the endothelium in acetylcholine-induced relaxation and spontaneous tone of bovine isolated retinal small arteries. *Exp Eye Res*. 1991;52:575–579.
8. Wu DM, Kawamura H, Sakagami K, Kobayashi M, Puro DG. Cholinergic regulation of pericyte-containing retinal microvessels. *Am J Physiol Heart Circ Physiol*. 2003;284:H2083–H2090.
9. Gericke A, Steege A, Manicam C, Bohmer T, Wess J, Pfeiffer N. Role of the m3 muscarinic acetylcholine receptor subtype in murine ophthalmic arteries after endothelial removal. *Invest Ophthalmol Vis Sci*. 2014;55:625–631.
10. Hoste AM, Andries LJ. Contractile responses of isolated bovine retinal microarteries to acetylcholine. *Invest Ophthalmol Vis Sci*. 1991;32:1996–2005.

11. Gould IG, Tsai P, Kleinfeld D, Linninger A. The capillary bed offers the largest hemodynamic resistance to the cortical blood supply. *J Cereb Blood Flow Metab*. 2017;37:52–68.
12. Hall CN, Reynell C, Gesslein B, et al. Capillary pericytes regulate cerebral blood flow in health and disease. *Nature*. 2014;508:55–60.
13. Nakazawa T, Kaneko Y, Mori A, et al. Attenuation of nitric oxide- and prostaglandin-independent vasodilation of retinal arterioles induced by acetylcholine in streptozotocin-treated rats. *Vascul Pharmacol*. 2007;46:153–159.
14. Horio N, Clermont AC, Abiko A, et al. Angiotensin at (1) receptor antagonism normalizes retinal blood flow and acetylcholine-induced vasodilatation in normotensive diabetic rats. *Diabetologia*. 2004;47:113–123.
15. Feit-Leichman RA, Kinouchi R, Takeda M, et al. Vascular damage in a mouse model of diabetic retinopathy: relation to neuronal and glial changes. *Invest Ophthalmol Vis Sci*. 2005;46:4281–4287.
16. Ivanova E, Kovacs-Oller T, Sagdullaev BT. Vascular pericyte impairment and connexin43 gap junction deficit contribute to vasomotor decline in diabetic retinopathy. *The J Neurosci*. 2017;37:7580–7594.
17. Sergeys J, Etienne I, Van Hove I, et al. Longitudinal in vivo characterization of the streptozotocin-induced diabetic mouse model: focus on early inner retinal responses. *Invest Ophthalmol Vis Sci*. 2019;60:807–822.
18. Sohn EH, van Dijk HW, Jiao C, et al. Retinal neurodegeneration may precede microvascular changes characteristic of diabetic retinopathy in diabetes mellitus. *Proc Natl Acad SciU S A*. 2016;113:E2655–E2664.
19. Martin PM, Roon P, Van Ells TK, Ganapathy V, Smith SB. Death of retinal neurons in streptozotocin-induced diabetic mice. *Invest Ophthalmol Vis Sci*. 2004;45:3330–3336.
20. Hammes HP, Lin J, Renner O, et al. Pericytes and the pathogenesis of diabetic retinopathy. *Diabetes*. 2002;51:3107–3112.
21. Yadav AS, Harris NR. Effect of tempol on diabetes-induced decreases in retinal blood flow in the mouse. *Curr Eye Res*. 2011;36:456–461.
22. Ivanova E, Alam NM, Prusky GT, Sagdullaev BT. Blood-retina barrier failure and vision loss in neuron-specific degeneration. *JCI Insight*. 2019;5:e126747.
23. Toychiev AH, Sagdullaev B, Yee CW, Ivanova E, Sagdullaev BT. A time and cost efficient approach to functional and structural assessment of living neuronal tissue. *J Neurosci Methods*. 2013;214:105–112.
24. Aarts E, Verhage M, Veenvliet JV, Dolan CV, van der Sluis S. A solution to dependency: using multilevel analysis to accommodate nested data. *Nat Neurosci*. 2014;17:491–496.
25. Zhao S, Ting JT, Atallah HE, et al. Cell type-specific channelrhodopsin-2 transgenic mice for optogenetic dissection of neural circuitry function. *Nat Methods*. 2011;8:745–752.
26. Iadecola C. The neurovascular unit coming of age: a journey through neurovascular coupling in health and disease. *Neuron*. 2017;96:17–42.
27. Ivanova E, Kovacs-Oller T, Sagdullaev BT. Domain-specific distribution of gap junctions defines cellular coupling to establish a vascular relay in the retina. *J Comp Neurol*. 2019;527:2675–2693.
28. Jing M, Zhang P, Wang G, et al. A genetically encoded fluorescent acetylcholine indicator for in vitro and in vivo studies. *Nat Biotechnol*. 2018;36:726–737.
29. Bi A, Cui J, Ma YP, et al. Ectopic expression of a microbial-type rhodopsin restores visual responses in mice with photoreceptor degeneration. *Neuron*. 2006;50:23–33.
30. Cehajic-Kapetanovic J, Eleftheriou C, Allen AE, et al. Restoration of vision with ectopic expression of human rod opsin. *Curr Biol*. 2015;25:2111–2122.
31. Baker CK, Flannery JG. Innovative optogenetic strategies for vision restoration. *Front Cell Neurosci*. 2018;12:316.
32. Wang Z, Yadav AS, Leskova W, Harris NR. Attenuation of streptozotocin-induced microvascular changes in the mouse retina with the endothelin receptor a antagonist atrasentan. *Exp Eye Res*. 2010;91:670–675.
33. Wright WS, Messina JE, Harris NR. Attenuation of diabetes-induced retinal vasoconstriction by a thromboxane receptor antagonist. *Exper Eye Res*. 2009;88:106–112.
34. Sarter M, Parikh V, Howe WM. Phasic acetylcholine release and the volume transmission hypothesis: time to move on. *Nat Rev Neurosci*. 2009;10:383–390.
35. Duong TQ, Ngan SC, Ugurbil K, Kim SG. Functional magnetic resonance imaging of the retina. *Invest Ophthalmol Vis Sci*. 2002;43:1176–1181.

Investigative Ophthalmology & Visual Science